Research Square

Preprints are preliminary reports that have not undergone peer review.
They should not be considered conclusive, used to inform clinical practice,
or referenced by the media as validated information.

Microplastics reshape lipid mediator responses in human iPSC-derived cardiomyocytes: polymer- and photo-oxidative aging-dependent effects

Denise Biagini
University of Pisa
Elisa Persiani
National Research Council
Antonella Cecchettini
National Research Council
Ilaria Gisone
National Research Council
Amel Ben Anes
University of Pisa
Silvia Ghimenti
University of Pisa
Andrea Corti
University of Pisa
Thierry Durand
Université de Montpellier
Camille Oger
Université de Montpellier
Fabio Di Francesco
University of Pisa
Valter Castelvetro
University of Pisa
Federico Vozzi
federico.vozzi@cnr.it
National Research Council
Tommaso Lomonaco
University of Pisa

Article

Keywords: Microplastics, hiPSC-derived cardiomyocytes, Lipid-mediators, Specialized pro-resolving mediators, Polyunsaturated fatty acids, Photo-oxidative aging.

Posted Date: November 17th, 2026

DOI: https://doi.org/10.21203/rs.3.rs-11409504/v1

License: This work is licensed under a Creative Commons Attribution 4.0 International License.
Read Full License

Additional Declarations: No competing interests reported.

Microplastics reshape lipid mediator responses in human iPSC-derived cardiomyocytes: polymer- and photo-oxidative aging-dependent effects

Denise Biagini[a§], Elisa Persiani[b§], Antonella Cecchettini[b,c], Ilaria Gisone[b], Amel Ben Anes[a], Silvia Ghimenti[a], Andrea Corti[a], Thierry Durand[d], Camille Oger[d], Fabio Di Francesco[a], Valter Castelvetro[a], Federico Vozzi[b*] and Tommaso Lomonaco*[a]

[a] Department of Chemistry and Industrial Chemistry, University of Pisa, Via Giuseppe Moruzzi 13, Pisa, Italy
[b] Institute of Clinical Physiology, National Research Council, Via Giuseppe Moruzzi 1, Pisa, Italy
[c] Biology Division, Department of Clinical and Experimental Medicine, University of Pisa, Pisa, Italy.
[d] Institut des Biomolécules Max Mousseron (IBMM), UMR 5247, Pôle Chimie Balard Recherche, Université de Montpellier, CNRS, ENSCM, France

§ Authors contributed equally to this work
* Co-corresponding Authors
Telephone: +39 050-621-2672
E-mail address: federico.vozzi@cnr.it
ORCID ID: 0000-0001-5457-2328

Suggested referees
Ref. 1: María Fernández Velasco (mfvlorenzo@gmail.com)
Ref. 2: Serena Ducoli (serena.ducoli@unibs.it)
Ref. 3: Angel Sanchez Illana (angel.illana@uv.es)

Highlights

- Validated LC-MS/MS platform for reliable lipid mediator profiling in cardiomyocytes
- Polymer chemistry and aging shape redox and inflammatory responses
- HDPE and PS induce the strongest oxidative/pro-inflammatory remodeling
- LDPE shows a polymer-state-dependent stress-response phenotype
- SPM and PUFA remodeling differ markedly across polymers

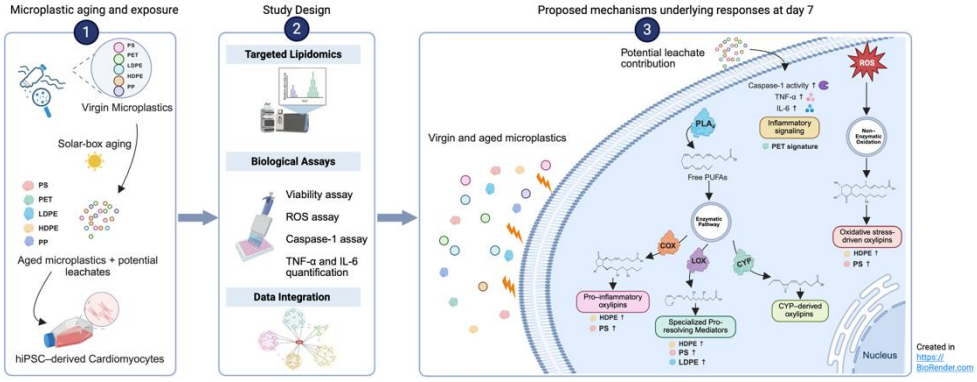
Abstract

Microplastics (MPs) are pervasive environmental contaminants detected in human cardiovascular tissues and associated with cardiovascular effects involving oxidative stress and inflammation. Oxylipins are key regulators of inflammatory signaling and cardiovascular homeostasis, yet the influence of MP polymer type and photo-oxidative aging on cardiomyocyte oxylipin profiles remains poorly characterized. Here, we combined targeted lipidomics using MEPS-UHPLC-MS/MS with cellular assays to investigate the polymer- and photo-oxidative aging-dependent effects of five common MPs, namely high-density polyethylene (HDPE), low-density polyethylene (LDPE), polystyrene (PS), polyethylene terephthalate (PET), and polypropylene (PP), in human induced pluripotent stem cell-derived cardiomyocytes (hiPSC-CMs) during a seven-day exposure. Fifty-six lipid mediators were longitudinally quantified in culture media, while cell viability, hydrogen peroxide, caspase-1 activity, and pro-inflammatory cytokines (IL-6 and TNF-α) were assessed at the endpoint. MP exposure induced distinct polymer- and aging-dependent lipid profiles. HDPE and PS exhibited the most pronounced oxidative and inflammatory oxylipin remodeling, whereas LDPE showed distinct aging-dependent profiles, with sustained elevations in polyunsaturated fatty acids (PUFAs) and specialized pro-resolving mediators (SPMs) after aging. PUFA increases were greatest with virgin HDPE and aged PS. SPM responses also varied across polymers, showing increases at late time points with HDPE and PS and sustained elevations with aged LDPE. Together, these findings identify polymer- and aging-dependent oxylipin remodeling as an underexplored dimension of the cardiomyocyte response to MP exposure and support differential coupling between lipid-redox remodeling and inflammatory signaling.

Keywords

Microplastics; hiPSC-derived cardiomyocytes; Lipid-mediators; Specialized pro-resolving mediators; Polyunsaturated fatty acids; Photo-oxidative aging.

Graphical Abstract



1. Introduction

Microplastics (MPs) are increasingly recognized as pervasive environmental contaminants with emerging implications for human health, including the cardiovascular system [1]. Consistent with systemic exposure, MPs have been detected in multiple human biological specimens, including blood [2], lung tissue [3], placenta [4], atherosclerotic plaques [5], and cardiac tissues, such as the myocardium, coronary arteries, and epicardial adipose tissue [6]. These findings support the potential relevance of MP exposure to cardiovascular tissues. *In vitro* studies further indicate that MP exposure promotes oxidative stress, inflammatory signaling, apoptosis, and endothelial dysfunction [7,8]. In contrast, animal models have demonstrated altered heart rate, impaired cardiac function, myocardial remodeling, fibrosis, and vascular injury following MP exposure [9].

Current knowledge of MP toxicity is largely derived from studies of pristine particles, most commonly polystyrene. It has relied predominantly on conventional endpoints such as reactive oxygen species (ROS) generation, cytokine release, and cytotoxicity. Consequently, little is known about whether different MP types elicit distinct biological responses in cardiovascular cells or how environmentally relevant aging processes influence their toxicity. Environmental aging therefore is a critical but often overlooked determinant of MP biological activity. Through photo-oxidation, chain scission, and the generation of oxygen-containing functional groups, aging alters polymer surface chemistry, creating distinct physicochemical fingerprints that can modify surface reactivity and biological behavior [8,10–13]. In addition to modifying particle surfaces, photo-oxidative aging can generate oxidized low-molecular-weight products and leachable compounds that may further influence biological responses. Together, these transformations may substantially affect MPs' ability to perturb redox-sensitive signaling pathways and downstream inflammatory responses. Rather than representing chemically inert debris, environmentally aged MPs should therefore be considered as chemically dynamic particulate systems with potentially distinct toxicological properties from their virgin counterparts.

Cardiomyocytes are particularly susceptible to perturbations in redox homeostasis and membrane integrity because of their sustained energy demand, high mitochondrial activity, and tightly regulated redox-lipid signaling networks [14,15]. As the principal functional cells of the myocardium, they integrate oxidative, inflammatory, and metabolic signals that govern cardiac adaptation to physiological and pathological stress. Given the detection of MPs in cardiac tissues and the central role of redox signaling in cardiomyocyte function, these cells represent a relevant model for investigating cellular mechanisms linking MP exposure, redox imbalance, and inflammatory signaling to cardiovascular injury [16]. Despite growing evidence of MP effects in vascular cells, comparatively little is known about their impact on cardiomyocytes, particularly with respect to redox-regulated lipid mediator signaling.

Among the molecular pathways linking oxidative stress and inflammation, lipid mediators derived from polyunsaturated fatty acids (PUFAs), including oxylipins such as specialized pro-resolving mediators (SPMs), play a central role [17,18]. Oxylipins are generated through enzymatic and non-enzymatic oxidation of PUFAs, linking redox imbalance to inflammatory signaling and regulating vascular function, immune responses, cell survival, and tissue repair [19]. SPMs actively promote inflammation resolution and restore tissue homeostasis, while dysregulation of pro-inflammatory and pro-resolving lipid mediator pathways has been implicated in cardiovascular disease [20]. Despite their biological relevance, lipid mediator responses remain poorly investigated in MP toxicology. Conventional biomarkers such as ROS and inflammatory cytokines provide only a partial view of cellular stress and inflammation, whereas comprehensive lipid mediator profiling can capture the interplay between oxidative damage, inflammatory activation, and endogenous resolution mechanisms [21]. Recent advances in targeted liquid chromatography–tandem mass spectrometry (LC-MS/MS) and miniaturized sample preparation enable sensitive quantification of low-abundance oxylipins and SPMs, providing a powerful approach to investigate lipid mediator remodeling under environmental and metabolic stress [22]. Given the dynamic nature of these responses, longitudinal

profiling is also important to distinguish transient adaptive changes from persistent inflammatory activation [23].

To date, no study has systematically examined how MP polymer chemistry and environmental aging influence oxylipin and pro-resolving lipid mediator networks in human cardiomyocytes. To address this gap, we used previously characterized virgin and photo-oxidatively aged MPs representing five common polymers, namely high-density polyethylene (HDPE), low-density polyethylene (LDPE), polystyrene (PS), polyethylene terephthalate (PET), and polypropylene (PP), during a seven-day exposure of human induced pluripotent stem cell-derived cardiomyocytes (hiPSC-CMs). At the end of the experimental period, markers of viability, inflammation (TNF-α, IL-6, caspase-1), and oxidative stress (H_2O_2) were analyzed to provide a preliminary evaluation of the MPs' effects. Then we tested the hypothesis that polymer-specific and aging-dependent changes in MP physicochemical properties differentially perturb redox-regulated lipid mediator pathways, leading to distinct inflammatory and resolution-associated responses. Using a validated platform combining microextraction by packed sorbent (MEPS) with ultra-high-performance liquid chromatography–tandem mass spectrometry (UHPLC-MS/MS), we longitudinally quantified PUFAs and oxylipins, including SPMs, and integrated these measurements with assessment of cell viability, ROS levels assessed by H_2O_2 measurement, caspase-1 activation, and cytokine release. By integrating mediator-level quantification with time-resolved pathway analysis, we aimed to identify polymer- and aging-specific signatures associated with redox imbalance, inflammatory activation, and resolution responses in cardiomyocytes, providing mechanistic insight into the cardiovascular effects of MP exposure.

2. Materials and methods

2.1. Chemicals and equipment

Acetonitrile (ACN), methanol (MeOH), and LC-MS-grade water (LiChrosolv®, purity ≥99.9%) were purchased from EMD Millipore (Milan, Italy). Butylated hydroxytoluene (BHT, purity ≥99%), formic acid (HCOOH, purity ≈98%), sodium tungstate dihydrate ($Na_2WO_4 \times 2H_2O$), and copper sulfate hexahydrate ($CuSO_4 \times 6H_2O$) were obtained from Merck (Milan, Italy).

Commercially available oxylipin standards (purity ≥99%), including isoprostanes, prostaglandins, thromboxanes, leukotrienes, lipoxins, resolvins, protectins, maresins, hydroxy- and epoxy-fatty acids, together with deuterated internal standards, were purchased from Cayman Chemical (Ann Arbor, MI, USA). Oxylipin standards not commercial available were synthesized at the Max Mousseron Institute of Biomolecules (IBMM, Montpellier, France) with a purity ≥98%, according to procedures reported elsewhere [24,25]. These included F_2-, F_3-isoprostanes, and F_4-neuroprostanes, F_2-dihomo-isoprostanes and isofurans, tetranor- and dinor- NPD1 metabolites, and dihydroxylated polyunsaturated fatty acid derivatives. All standards were stored at -80 °C in amber vials and thawed on ice before use.

Sterile polypropylene tubes were purchased from Eppendorf (Milan, Italy), and Phenex™-RC syringe filters (0.2 µm regenerated cellulose, 4 mm diameter) were obtained from Phenomenex (Torrance, CA, USA). A ZX4 Advanced vortex mixer was purchased from VELP Scientifica (Usmate, Italy), and a benchtop centrifuge was obtained from Benchmark Scientific Inc. (Sayreville, NJ, USA). Automated MEPS was performed on an HTA300APlus system from HTA S.r.l. (Brescia, Italy) equipped with a 250 µL analytical syringe and a BIN C18 cartridge from SGE Analytical Science (Melbourne, Australia).

2.2. Preparation of standard solutions and quality control samples

Stock and working standard solutions of PUFAs, oxylipins, and their corresponding deuterated internal standards (ISs) were prepared following previously established procedures [21]. Working standard solutions were used to generate five-point calibration curves covering the expected concentration range in cell culture media. Working solutions were prepared fresh each month and

stored at -80 °C.

Pooled matrix samples were obtained by combining equal aliquots of experimental media from untreated and treated cardiomyocyte cultures. Quality control (QC) samples were prepared by spiking the pooled matrix with intermediate standard solutions to achieve low, medium, and high concentration levels, corresponding to the first, third, and fifth points of the calibration range. The total volume of spiked solution did not exceed 10% of the matrix volume to preserve matrix integrity.

2.3 Microplastic features and aging procedure

Cryogenically micronized PS (nominal density 1.05 g/cm³, mean particle size of 564 µm), HDPE (density 0.952 g/cm³, mean particle size of 622 µm), LDPE (density 0.917 g/cm³, mean particle size of 632 µm), PP (nominal density 0.900 g/cm^3, mean particle size of 857 µm), and PET (about 5 % crystallinity as provided, nominal density 1.28 g/cm^3, mean particle size of 509 µm) were kindly provided by Poliplast S.p.A. (Casnigo, Italy). Virgin polymer powders were exposed to accelerated photo-oxidative aging for four weeks in a solar-box chamber equipped with an Xe lamp to promote radical-mediated oxidative degradation, according to a previously described protocol [14]. Aged polymers were stored at -20 °C in amber glass vials to limit uncontrolled oxidative processes and equilibrated at room temperature (25 ± 2 °C) before their use. Materials were sterilized with three consecutive UV irradiation cycles, each lasting 15 min. Full chemical and physicochemical characterization of these polymers, including oxidation indices and particle size distribution, was reported elsewhere [13].

2.4 Cell culture and microplastic exposure

For biological experiments, all cell culture materials were supplied by Thermo Fisher Scientific (Waltham, MA, USA).

Human-hiPSCs (hiPSCs) bwere cultured on vitronectin-coated flasks in Essential 8® Flex basal medium with supplement and 1% Penicillin/Streptomycin (P/S). The medium was refreshed every 2 days, and at 70%–80% confluence, cells were gently passaged using Versene without disrupting cell clusters. Cell seeding density was 20,000 cells/cm^2.

For differentiation, hiPSCs (70%–80% confluence) were rinsed twice with Dulbecco's phosphate-buffered saline (DPBS) without calcium and magnesium (DPBS −/−), then detached and dissociated into single cells with TrypLE. Cells were seeded in VTN-N-coated flasks (seeding density of 20,000 cells/cm^2), and the medium was replaced every 2 days until 50%–60% confluence was reached. Then, the differentiation protocol started and continued for 12 days using the PSC Cardiomyocyte Differentiation Kit, following the manufacturer's instructions [26]. On day 12, hiPSC-CMs were dissociated with Versene and seeded into 96-well plates at a density of 20,000 cells/cm^2 for MP treatment. Polymer suspensions were freshly prepared in supplemented Maintenance Medium to a final concentration of 1 mg/mL, and cells were treated with the different MPs for 7 days. Aliquots were withdrawn while maintaining the dispersion under constant agitation. This concentration was selected to ensure compatibility with the assessment of oxidative stress and redox-dependent cellular responses [27]. For oxylipin profiling, culture media samples were collected after 2, 4, and 7 days of incubation in dedicated Eppendorf tubes containing a 15 mg/mL methanolic solution of BHT to prevent ex vivo oxidation [28], then quickly stored at -80 °C before analysis on the LC-MS/MS platform. Biological readouts were performed at the end of the 7-day exposure period.

2.5 Cell viability

Cell viability was assessed using the CellTiter-Blue® Cell Viability Assay (Promega, Madison, WI, USA). Briefly, viable cells reduce resazurin to resorufin, generating a fluorescence signal proportional to the number of metabolically active, viable cells. To perform the viability assay, 20 µL of CellTiter-Blue® reagent were added to each well of a 96-well plate containing 100 µL of medium. The samples were incubated at 37 °C for 2.5h. Fluorescence was measured at excitation and emission wavelengths of 560 nm (Ex) and 590 nm (Em), respectively, using a Fluostar Omega

spectrofluorimeter (BMG Labtech, Ortenberg, Germany).

2.6 Oxidative stress

H_2O_2 levels were measured as an indicator of oxidative stress using the ROS-Glo™ H_2O_2 Assay Kit (Promega, Madison, WI, USA). Samples were processed according to the manufacturer's instructions. Briefly, 20 µL/well of the H_2O_2 substrate solution was added to each sample, then incubated for 3 hours at 37 °C. Then, 50 µL/well of cell culture medium was transferred to a white, opaque 96-well plate and mixed with 50 µL/well of ROS-Glo™ Detection Solution. After a 20-minute incubation at room temperature in the dark, relative luminescence units (RLU) were measured using a luminometer.

2.7 Caspase-1

To assess caspase-1 activity in culture media from treated cells, the Caspase-Glo®-1 Inflammasome Assay Kit (Promega, Madison, WI, USA) was used according to the manufacturer's instructions. An aliquot (20 µL) of cell culture medium was transferred to a white, opaque 96-well plate. Samples were then treated with 50 µL/well of Caspase-Glo®-1 Reagent (for caspase-1 detection). Samples were incubated at room temperature for 1 hour and protected from light. Luminescence was measured using a luminometer and expressed in relative luminescence units (RLU).

2.8 Cytokines

IL-6 was measured using an automated ELISA system (Elecsys® IL-6, Roche Diagnostics, Basel, Switzerland). The Roche Elecsys IL-6 assay is a non-competitive chemiluminescent immunoassay. An aliquot (30 µL) of each sample was first incubated with anti-IL-6 antibodies, then incubated with ruthenium-labeled anti-IL-6 antibodies. The resulting complexes were magnetically captured, generating a chemiluminescent emission signal directly proportional to the IL-6 concentration in the medium. The limit of detection (LOD) is 1.5 pg/mL, the detection range is 1.5-20 pg/mL, and the intra-assay and inter-assay variability are <3% and <5%, respectively. For TNF-α detection, the Human TNF-α ELISA kit (Thermo Fisher Scientific, Waltham, Massachusetts, USA) was used according to the manufacturer's instructions. Briefly, 50 µL of cell supernatant was incubated in a 96-well plate coated with immobilized monoclonal anti-TNF-α antibodies. Subsequently, biotin-conjugated anti-TNF-α antibodies and streptavidin peroxidase were added to each well. The antibody-protein complex was then detected by adding the chromogenic substrate (tetramethylbenzidine), and the absorbance was measured at 450 nm. The LOD for human TNF-α is 0.13 pg/mL, the detection range is 0.31-20 pg/mL, and the intra-assay and inter-assay variability are 8.5% and 9.8%, respectively.

2.9 Oxylipins and PUFAs profiling

Cell culture media samples were analyzed using an adapted MEPS-UHPLC-MS/MS workflow originally developed for determining oxylipins and PUFAs in biological matrices [29,30] and subsequently extended to culture media. Briefly, before extraction, media samples (500 µL) were spiked with 20 µL of an IS mixture (20 ng/mL) and subjected to protein removal using sequential addition of $CuSO_4 \times 6H_2O$ (250 µL, 10% w/v), $Na_2WO_4 \times 2H_2O$ (250 µL, 12% w/v), and ACN (500 µL). Samples were vortex-mixed (2000 rpm for 1 min), centrifuged (7000 rpm for 5 min), filtered (0.2 µm), and diluted five-fold with water before MEPS-based clean-up. C18 MEPS cartridges were conditioned with methanol and water (0.6 mL/min, three draw/discharge cycles using 100 µL for each solvent). The diluted supernatant (3000 µL) was loaded and eluted 12 times at 0.3 mL/min in discarding mode to retain analytes. After washing with 100 µL of water:methanol (95:5 v/v) at 0.6 mL/min to remove potential interferences, analytes were eluted in 50 µL of methanol at 0.3 mL/min and then injected into the UHPLC-MS/MS system.

Chromatographic separation was carried out using an Agilent 1290 Infinity II LC system with a

Polaris 3 C18-A column (50 × 4.6 mm, 3 μm, Agilent Technologies, USA), using a gradient of 0.1% aqueous formic acid (A) and methanol:acetonitrile (50:50 v/v, B), with the proportion of B increased from 10% to 80% over 26 min at a flow rate of 0.7 mL/min. The multisampler and the column compartment were set at 4 °C and 25 °C, respectively. The injection volume was 20 μL. Detection was performed on an Agilent 6495 Triple Quadrupole mass spectrometer with ESI negative ionization mode in multiple reaction monitoring (MRM) with unit mass resolution. For each analyte, the most intense transition (Q) was used for quantification, and a secondary transition (q) served as the qualifier. Compound identity was confirmed by retention time (±0.10 min) and by the qualifier-to-quantifier (q/Q) ratio (±20%) relative to reference standards (Table S1). Instrumental control, data acquisition and processing were performed using the MassHunter Workstation software (B.07.00). Detailed chromatographic parameters, ESI conditions, and MRM operating conditions are reported elsewhere [29,30].

2.10 Method validation for oxylipin profiling in cell culture media

Analytical figures of merit were evaluated in accordance with IUPAC guidelines [31], including limits of detection (LOD) and quantification (LOQ), linearity, matrix effect, recovery, and intra-day and inter-day precision. Detection and quantification limits were calculated as three and ten times the standard deviation of low-level fortified blank matrix samples, respectively. Calibration curves were generated from five concentration points in both solvent and pooled matrix, with triplicate measurements per level. The ratio of analyte peak area (a) to internal standard (IS) peak area ($Y=A_a/A_{IS}$) was plotted against the corresponding concentration ratio ($X=C_a/C_{IS}$), and the Deming regression model ($Y=mX$) was applied to account for uncertainties in both variables [32]. Linearity was verified by inspecting residuals and evaluating goodness-of-fit metrics. Matrix effects were assessed by comparing solvent-based and matrix-matched slopes across the calibration range at a 95% confidence level. Matrix-matched calibration was applied when a significant matrix effect was observed. Extraction recovery was evaluated at low, medium, and high concentration levels in triplicate on a single day (intra-day) and across three consecutive days (inter-day). Recovery was expressed as the percentage of analyte retrieved relative to the spiked amount. Intra- and inter-day precision were reported as the relative standard deviation (RSD) of measurements performed on spiked samples (n=3).

2.11 Statistical analysis

Variables detected in fewer than 50% of samples were excluded from statistical analysis to minimize the influence of sparsely detected features and improve the robustness of statistical inference [33]. For the remaining analytes, values below the LOD were imputed with random values between 0 and the minimum observed concentration, a conservative approach commonly used to preserve data structure while limiting artificial variance inflation [34]. Data distribution was assessed using the Shapiro-Wilk test, and a $\log_{10}$ transformation was applied when necessary to reduce skewness [35].

To assess class-level oxylipin remodeling, individual analytes were assigned to four predefined functional classes: (i) oxidative products generated by non-enzymatic PUFA peroxidation (including isoprostanes, isofurans, and related species), (ii) pro-inflammatory cyclooxygenase (COX)/5-lipoxygenase (5-LOX)-derived mediators (including prostaglandins and leukotrienes), (iii) PUFAs (arachidonic acid [AA], eicosapentaenoic acid [EPA], docosahexaenoic acid [DHA], and docosapentaenoic acid [DPA]), and (iv) SPMs, including resolvins, protectins, maresins, and lipoxins. For each analyte, abundance in exposed samples was normalized to the corresponding time-matched control and expressed as the Log_2 fold change (Log_2FC), calculated as Log_2 (exposed/control). For each polymer, aging condition, and time point, analyte-level Log_2FC values were averaged within each functional class to generate a class-level mean Log_2FC, which was used for descriptive comparisons across conditions.

Temporal and group-wise effects were analyzed using linear mixed-effects models, with time,

microplastic type, aging, and their interactions included as fixed effects, and a random intercept for each biological replicate [35]. Random slopes were applied when pronounced temporal trends were observed. Model assumptions were assessed by inspecting residuals and evaluating homoscedasticity. When the overall model indicated significant effects, post hoc pairwise comparisons were performed using estimated marginal means, with p-values adjusted for multiple testing using the Benjamini–Hochberg false discovery rate (FDR) procedure. For variables that did not satisfy parametric assumptions after transformation, non-parametric analyses were applied as appropriate. Homogeneity of variance was assessed using Levene's test. Associations among metabolites were assessed using Pearson or Spearman correlations, depending on the variable distribution. Correlation strength was interpreted as weak ($|r| \geq 0.1$), moderate ($|r| \geq 0.3$), or strong ($|r| \geq 0.5$). P-values were adjusted for multiple testing using the Benjamini–Hochberg procedure [36].

Pathway-based network visualizations were generated using Cytoscape version 3.10.4 (https://cytoscape.org; accessed on 15 June 2026) [37]. Oxylipin metabolic networks were constructed based on established PUFA-derived biosynthetic pathways, including lipoxygenase (LOX)-, COX-, cytochrome P450 (CYP)-, and ROS-mediated reactions. Metabolites were represented as nodes and mapped according to their Log_2FC to visualize polymer- and aging-dependent remodeling of lipid mediator pathways.

Visualization was performed using GraphPad Prism version 11.0 (GraphPad Software, San Diego, CA, USA). A two-tailed p-value <0.05 was considered statistically significant. All data processing and statistical analyses were performed in RStudio (Boston, USA) using appropriate packages.

3. Results

3.1. Analytical figures of merit

The analytical protocol was evaluated for the simultaneous and reliable quantification of fifty-six lipid analytes in cell culture media (Table 1). Limits of detection ranged from 7 to 922 pg/mL for oxylipins and from 0.3 to 2.7 ng/mL for PUFAs, allowing trace-level detection in complex media. Accuracy was assessed at three QC levels (low, medium, and high) across the calibration range. For most oxylipin classes, recovery values ranged from 78% to118% for intra-day assessments and from 79% to 121% for inter-day assessments. Lower recoveries were observed for SPMs and F_{2t}-dihomo-isoprostanes (F_{2t}-dihomo-IsoPs), ranging from approximately 45% to 80% in both intra- and inter-day analyses. Despite the lower recovery observed for SPMs, this did not represent a limitation for comparative analyses, as recoveries were consistent and reproducible across samples. Further methodological optimization may, however, improve extraction efficiency and sensitivity in culture media for these low-abundance mediators. Relative precision was consistently below 20%, and no statistically significant differences were observed among the different QC levels. Linearity was confirmed using five-point calibration curves, providing coefficients of determination (R^2) between 0.95 and 1.00 across the investigated range. Matrix effects were evaluated by ANOVA comparing calibration slopes in water and in cell culture media from cardiomyocyte cultures, with or without virgin and/or aged MPs, using a significance threshold of $p < 0.05$ (two-tailed). Most analytes exhibited comparable responses across matrices, indicating limited overall matrix interference. However, several D-series resolvins (e.g., Resolvin D2, 17(R)-Resolvin D1, and Resolvin D4/17(R)-Resolvin D4), lipoxins (Lipoxin A4 and B4), protectins (Tetranor-Neuroprotectin D1 and Protectin DX), and selected dihydroxyeicosatetraenoic acids (14,15-DiHETE, 11,12-DiHETE, 8,9-DiHETE) and hydroxyeicosatetraenoic acids (15-HETE) displayed significant signal enhancement in culture media compared to water. In contrast, some precursor PUFAs, including EPA, DHA, and AA, showed reduced responses consistent with ion suppression. These data support the use of matrix-matched calibration is recommended to ensure accurate quantification of susceptible analytes.

Table.1 Retention time, limits of detection (LODs), intra-day and inter-day recovery for the determination of oxylipins in cell culture media.

Compound	Retention time (min)	Internal standard	LOD (pg/mL)	Recovery (%) (RSD*)	
				Intra-day	Inter-day
Resolvin E1	6.14	Resolvin D1-d5	16	100(16)	96(17)
8-F_{3t}-IsoP	6.27	C21 15-F_{2t}-IsoP	15	82(7)	90(8)
18-F_{3t}-IsoP	6.73	C21 15-F_{2t}-IsoP	34	95(19)	85(21)
8-*epi*-8-F_{3t}-IsoP	6.85	C21 15-F_{2t}-IsoP	37	78(7)	85(10)
15-F_{2t}-IsoP	7.99	15-F_{2t}-IsoP-d4	13	94(8)	92(12)
20-*epi*-20-F_{4t}-NeuroP	8.16	10-*epi*-F_{4t}-NeuroP-d4	203	89(20)	85(17)
TXB2	8.19	15-F_{2t}-IsoP-d4	53	104(6)	98(12)
5-F_{2t}-IsoP	8.24	15-F_{2t}-IsoP-d4	66	110(4)	102(10)
5-*epi*-5-F_{2t}-IsoP	8.39	15-F_{2t}-IsoP-d4	63	118(7)	114(14)
14(*R,S*)-14-F_{4t}-NeuroP(1)	8.51	10- F_{4t}-NeuroP- d4	192	88(15)	89(15)
20-F_{4t}-NeuroP	8.56	10- F_{4t}-NeuroP- d4	89	88(18)	85(16)
15-E_{2t}-IsoP	8.54	15-E_{2t}-IsoP-d4	7	80(14)	86(21)
14(*R,S*)-14-F_{3t}-NeuroP	8.61	10- F_{4t}-NeuroP- d4	34	93(6)	93(9)
Tetranor-Neuroprotectin D1	8.65	Maresin 1-d5	13	75(2)	71(8)
14(*R,S*)-14-F_{4t}-NeuroP(2)	8.66	10- F_{4t}-NeuroP-d4	110	83(22)	78(19)
17(*R*)-Resolvin D3	8.87	17(*R*)-Resolvin D1-d5	23	64(18)	71(19)
Lipoxin B4	8.89	Lipoxin A4-d5	12	51(7)	57(12)
PGE2	8.95	PGE2-d4	8	65(13)	63(19)
Resolvin D3	8.96	Resolvin D1-d5	26	54(9)	54(15)
Resolvin D2	9.10	Resolvin D1-d5	10	60(22)	64(16)
4(*R,S*)-4-F_{4t}-NeuroP	9.19	10- F_{4t}-NeuroP-d4	17	100(9)	92(11)
PGD2	9.17	PGE2-d4	14	79(18)	75(16)
Resolvin D1	9.58	Resolvin D1-d5	16	51(17)	51(19)
Lipoxin A4	9.59	Lipoxin A4-d5	13	46(10)	50(11)
7(*R,S*)-ST-$\Delta^{8\text{-}11}$-dihomo-IsoF	9.71/9.84	17(*R*)-Resolvin D1-d5	93	47(15)	44(22)
17(*R*)-Resolvin D1	9.72	17(*R*)-Resolvin D1-d5	16	49(14)	53(17)
ent-7(*R,S*)-7-F_{2t}-dihomoIsoP	9.85/10.02	17(*R*)-Resolvin D1-d5	25	68(9)	75(9)
16(*S*),9(*R*)-linotrin	9.88	Maresin 1-d5	10	74(10)	72(14)
17-F_{2t}-dihomoIsoP	10.09	17(*R*)-Resolvin D1-d5	47	75(4)	79(11)
Resolvin D4/17(*R*)-Resolvin D4	10.44	Resolvin D1-d5	14	82(2)	77(7)
dinor-Neuroprotectin D1	10.56	Maresin 1-d5	55	73(11)	79(15)
7-*epi*-maresin-1	11.28	Maresin 1-d5	68	102(7)	98(15)
diH-$DPA_{n\text{-}3}$	11.49	Maresin 1-d5	51	95(5)	100(12)
Protectin DX	11.61	Maresin 1-d5	17	76(13)	85(15)
Resolvin D5	11.66	Maresin 1-d5	32	78(9)	84(14)
Neuroprotectin D1	11.77	Maresin 1-d5	35	99(18)	116(19)
Maresin-1	11.87	Maresin 1-d5	63	94(15)	106(14)
14,15-DiHETE	12.10	Maresin 1-d5	60	90(14)	95(15)
11,12-DiHETE	12.15	Maresin 1-d5	43	75(13)	88(15)
LTB4	12.15	Maresin 1-d5	154	115(10)	108(18)
8,9-DiHETE	12.37	Maresin 1-d5	43	80(10)	79(13)
Maresin-2	12.51	Maresin 1-d5	87	95(12)	91(19)
diH-$DPA_{n\text{-}6}$	12.60	Maresin 1-d5	14	92(13)	84(16)
diH-AdA	12.97	Maresin 1-d5	153	94(7)	111(13)
20-HETE	13.99	20-HETE-d6	35	98(15)	85(11)
13-HODE	14.36	20-HETE-d6	922	77(18)	79(14)
15-HETE	14.40	20-HETE-d6	20	109(21)	94(19)
12-HETE	14.84	20-HETE-d6	31	109(17)	101(20)
5-HETE	15.38	20-HETE-d6	42	115(19)	121(20)
14,15-EET	15.54	14,15-EET-d11	45	81(15)	83(17)
11,12-EET	16.05	14,15-EET-d11	32	87(19)	91(14)
8,9-EET	16.26	14,15-EET-d11	37	81(8)	88(11)
EPA*	18.35	LA-d4	2.7	110(17)	107(21)
DHA*	19.74	LA-d4	1.9	111(20)	109(19)
AA*	20.45	LA-d4	1.8	117(19)	113(20)
DPA*	21.05	LA-d4	0.3	102(16)	121(15)

*LOD in ng/mL

3.2. Polymer-specific effects on cardiomyocyte viability, oxidative stress, caspase-1 activity, and cytokine responses after 7-day exposure

Following exposure, cardiomyocyte viability, as assessed by the CellTiter-Blue assay, significantly decreased only in response to aged LDPE (38% decrease *vs.* control) and increased with aged PS (61% increase *vs.* control), whereas no significant differences were observed for HDPE, PP, and PET, regardless of aging status (Figure 1A). ROS levels, assessed by H_2O_2 measurement, showed a broader response pattern (Figure 1B). Exposure to both virgin and aged HDPE and LDPE, as well as virgin PS, significantly increased ROS levels relative to controls, with fold changes of 3.6, 3.4, 3.2, and 1.9 for virgin HDPE, virgin LDPE, aged LDPE, and virgin PS, respectively. Aged PS did not significantly alter ROS levels. In contrast, PP and PET did not significantly affect ROS level. Caspase-1 activity varied across polymer types and aging conditions (Figure 1C). HDPE and PET significantly increased caspase-1 activity in both virgin and aged forms, whereas LDPE significantly increased caspase-1 activity only in its virgin form and PP only in its aged form. PS exposure did not significantly alter caspase-1 activity compared with controls. Pro-inflammatory cytokine profiles also varied according to polymer type. TNF-α levels increased following exposure to LDPE, PP, and PET irrespective of aging status, while HDPE and PS had no significant effect (Figure 1D). IL-6 responses were more heterogeneous (Figure 1E). PET exposure resulted in approximately two-fold increases in IL-6 levels, reaching 2.2 and 2.5 times the control values for virgin and aged particles, respectively. Conversely, HDPE reduced IL-6 levels regardless of aging status, whereas a decrease was observed only with virgin PS.

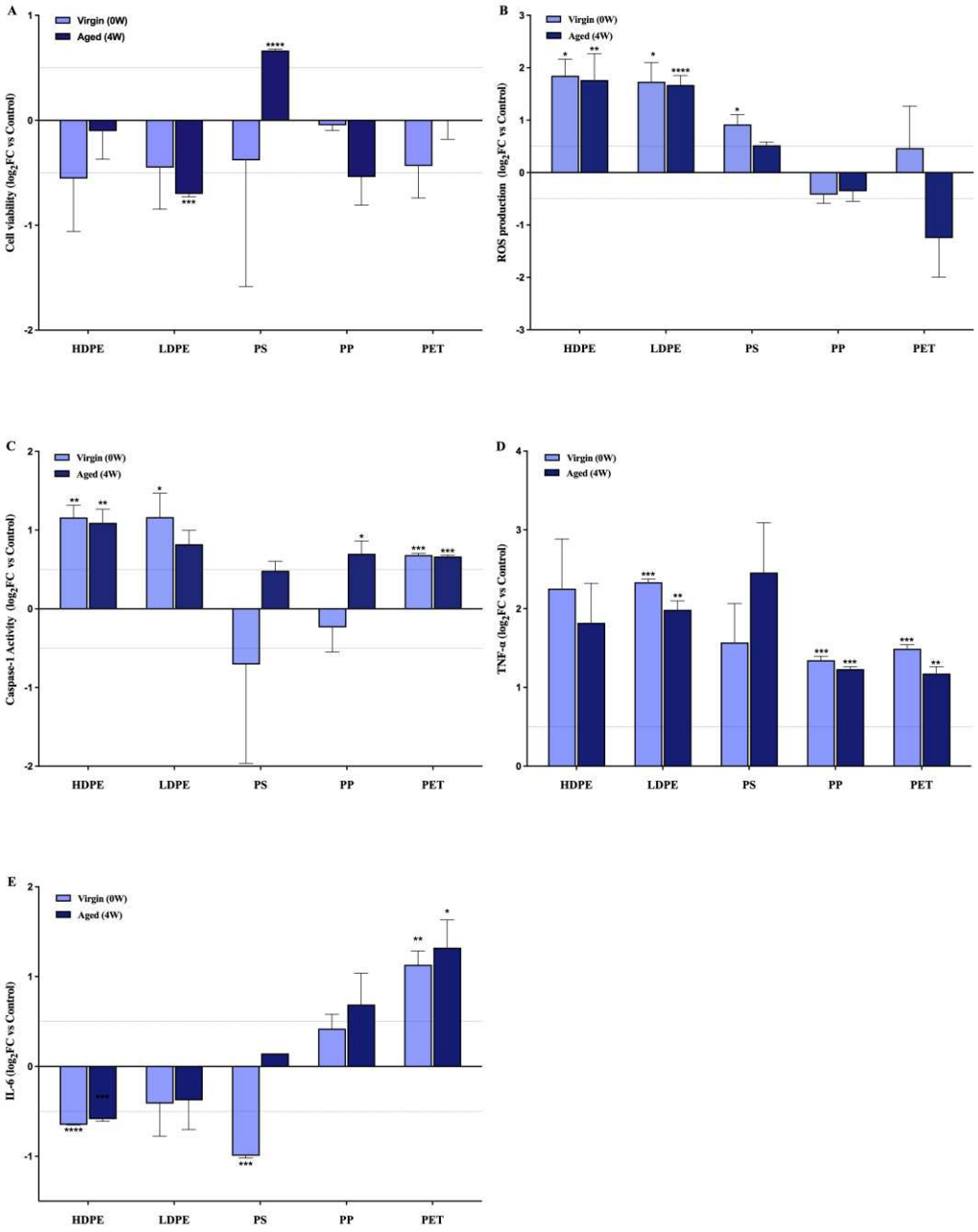


Figure 1. Effects of virgin (0W) and aged (4W) microplastics (HDPE, LDPE, PS, PP, and PET) on cell viability (A), ROS production (B), Caspase-1 activity (C), TNF-α (D), and IL-6 (E) after 7 days. Data are expressed as Log_2 FC relative to the corresponding control. Bars show mean ± SD; n = 3 per group. *p < 0.05, **p < 0.01, ***p < 0.001, and ****p < 0.0001.

3.3 Time-dependent lipid mediator dynamics: pro-inflammatory oxylipin activation induced by virgin and aged MPs

Changes in pro-inflammatory oxylipin levels were observed across all MPs, with clear polymer-specific differences in magnitude and temporal progression (Table 2). Among virgin materials, HDPE and PS caused the most pronounced time-dependent increases, with mean log_2 FC values rising markedly from day 2 to day 7 (HDPE: 0.5 to 3.2 and PS: 0.1 to 2.1). Virgin PP caused a more moderate but progressive increase over time, whereas virgin LDPE induced a transient response, peaking at day 4 (1.8) before declining at day 7 (0.4). In contrast, with PET, the values remained relatively stable across all time points (approximately0.5–0.6). Aging modulated these profiles in a polymer-dependent manner. Aged PS showed the strongest late-phase response, reaching the highest pro-inflammatory level at day 7 (Log_2 FC of 4.8). Aged HDPE and PP displayed weaker time-

dependent responses than their virgin counterparts, while aged LDPE retained a transient response with reduced late-phase amplitude. PET was largely unaffected by aging. Single-mediator mixed-effects modeling identified a significant increase in prostaglandin E_2 (PGE_2) between day 2 and day 7 ($p < 0.05$).

Table 2. Log_2 FC values for the pro-inflammatory oxylipins in cardiomyocyte media exposed to virgin and aged microplastics for 2, 4, and 7 days. Log_2 FC was calculated as the ratio of exposed samples to controls. The pro-inflammatory profile was derived from predefined COX/5-LOX-derived mediators included in the panel.

Polymer	Aging	Time (days)		
		2	4	7
PET	Virgin	0.6	0.5	0.6
	Aged	0.5	0.4	0.6
PP	Virgin	0.5	0.7	1.2
	Aged	0.1	0.2	0.6
HDPE	Virgin	0.5	1.8	3.2
	Aged	0.5	1.6	2.2
LDPE	Virgin	0.6	1.8	0.4
	Aged	0.6	1.7	0.9
PS	Virgin	0.1	0.8	2.1
	Aged	0.1	1.0	4.8

3.4 Polymer-dependent oxidative stress-driven oxylipin remodeling

All MPs were associated with measurable oxidative stress-driven oxylipin production, with marked differences across polymers in both magnitude and temporal evolution (Table 3). Among virgin materials, HDPE and PS exhibited the most pronounced time-dependent increases, rising from low initial levels at day 2 to substantially elevated values at day 7 (Log_2 FC HDPE: 0.2 to 1.5; PS: 0.6 to 1.7). Virgin LDPE also showed a progressive increase, reaching a Log_2 FC of 1.3 at day 7, whereas virgin PP displayed a limited early response followed by a moderate increase at the final time point. In contrast, PET remained comparatively stable across the exposure period, with values remaining close to a Log_2 FC of 1.0. Aging altered oxidative responses in a polymer-specific manner. Aged HDPE and aged PS showed the strongest late-phase increases, both reaching the highest oxidative levels observed (Log_2 FC of 2.7 at day 7). Aged LDPE and aged PP exhibited more moderate but consistent increases over time, whereas aged PET showed only a modest late change, maintaining an overall stable profile. Consistent with these class-level trends, mixed-effects modeling identified significant time-dependent increases in selected isoprostane (IsoP)/isofuran(IsoF) species under polymer- and aging-specific conditions associated with stronger oxidative responses ($p < 0.05$).

Table 3. Log_2 FC values for the oxidative oxylipin profile in cardiomyocyte media exposed to virgin and aged microplastics for 2, 4, and 7 days. Log_2 FC was calculated as the ratio of exposed samples to controls. The oxidative profile included non-enzymatic products of PUFA peroxidation.

Polymer	Aging	Time (days)		
		2	4	7
PET	Virgin	1.0	0.9	0.9
	Aged	0.8	0.9	1.2
PP	Virgin	0.3	0.3	0.8
	Aged	0.5	0.6	1.2
HDPE	Virgin	0.2	0.6	1.5
	Aged	0.3	0.7	2.7
LDPE	Virgin	0.5	0.8	1.3
	Aged	0.8	1.2	1.7
PS	Virgin	0.6	1.3	1.7
	Aged	0.9	1.7	2.7

3.5 SPM responses reveal uncoupling from inflammatory resolution

All MPs were associated with measurable changes in the SPM profile, with pronounced polymer- and aging-dependent differences in magnitude and temporal progression (Table 4). Among virgin materials, HDPE and PS exhibited the most marked late-phase increases, with mean Log_2 FC values rising from low or moderate levels at day 2 to peak values at day 7 (HDPE: 0.2 to 4.2; PS: 2.7 to 4.2). Virgin LDPE showed a moderate increase over time (up to 1.6), whereas virgin PP displayed a delayed response, with limited changes at early time points followed by an increase at day 7. In contrast, PET remained relatively stable across all time points, with values close to 1.0. Aging further modified these temporal patterns. Aged HDPE and aged PS showed strong late-phase responses, reaching mean Log_2 FC values of 3.5 and 3.0, respectively, at day 7. Aged LDPE exhibited sustained elevations across all time points (2.0–2.9), while aged PP showed only modest temporal variation. Consistent with observations in other pathways, PET displayed minimal sensitivity to aging, maintaining a relatively stable SPM profile. Notably, increases in SPM levels occurred in parallel with sustained elevations in pro-inflammatory and oxidative stress-driven oxylipins. Thus, although SPM levels were markedly elevated, particularly with HDPE and PS, these changes were not associated with reduced pro-inflammatory mediator levels at later time points, suggesting concurrent elevations in pro-resolving and pro-inflammatory mediators.

Table 4. Log_2 FC values for the SPMs oxylipin profile in cardiomyocyte media exposed to virgin and aged microplastics for 2, 4, and 7 days. Log_2 FC was calculated as the ratio of exposed samples to controls. The SPM profile was derived from specialized pro-resolving mediators, including resolvins, protectins, maresins, and lipoxins.

Polymer	Aging	Time (days)		
		2	4	7
PET	Virgin	1.0	1.2	1.1
	Aged	1.2	0.9	1.0
PP	Virgin	0.8	0.6	2.1
	Aged	1.3	0.9	1.2
HDPE	Virgin	0.2	1.9	4.2
	Aged	1.1	1.9	3.5
LDPE	Virgin	0.8	0.8	1.6
	Aged	2.0	2.3	2.9
PS	Virgin	2.7	1.7	4.2
	Aged	2.0	1.9	3.0

3.6 PUFA remodeling and availability

PUFA levels showed clear polymer- and aging-dependent temporal patterns (Table 5). Virgin HDPE showed the strongest increase in mean log_2 FC, from 0.1 at day 2 to 4.8 at day 7, while LDPE peaked at 3.4 on day 4 before declining to 0.6. PP increased progressively from 0.2 to 1.4, whereas PS and PET remained relatively stable. Aging markedly reshaped these profiles: aged PS increased from 0.2 to 4.3, aged HDPE reached 3.8 at day 7, and aged LDPE remained elevated (1.4,3.2, and2.5 at days 2, 4, and 7, respectively). PET was minimally affected by aging. Mixed-effects models identified significant increases in selected PUFAs in following exposure to HDPE (AA, DHA, and n-3DPA) and LDPE (EPA, DHA), particularly at day 7.

Table 5. Log_2 FC values for PUFA production in cardiomyocyte media exposed to virgin and aged microplastics for 2, 4, and 7 days. Log_2 FC was calculated as the ratio of exposed samples to controls.

Polymer	Aging	Time (days)		
		2	4	7
PET	Virgin	0.4	0.7	0.5
	Aged	0.4	0.8	0.6
PP	Virgin	0.2	1.2	1.4
	Aged	0.7	0.9	1.7
HDPE	Virgin	0.1	3.8	4.8
	Aged	0.6	2.9	3.8
LDPE	Virgin	0.2	3.4	0.6
	Aged	1.4	3.2	2.5
PS	Virgin	0.1	0.8	0.9
	Aged	0.2	1.7	4.3

3.7 Material-dependent alterations in oxylipin and specialized pro-resolving mediator networks

Network analysis revealed distinct, time-dependent alterations in lipid mediator profiles following MP exposure (Figure 2; Supplementary Figure S1). PS induced the most extensive remodeling, characterized by progressive increases in both n-6 PUFA-derived oxylipins and n-3 PUFA-derived SPMs, with the strongest effects observed at day 7. In contrast, PET produced fewer and less marked changes across both lipid networks. HDPE and LDPE showed intermediate effects, while PP elicited comparatively modest alterations. Across all materials, lipid mediator responses were generally more pronounced at day 7, while the impact of material aging varied among individual metabolites, indicating that both polymer type and aging status modulate lipid mediator profiles over time.

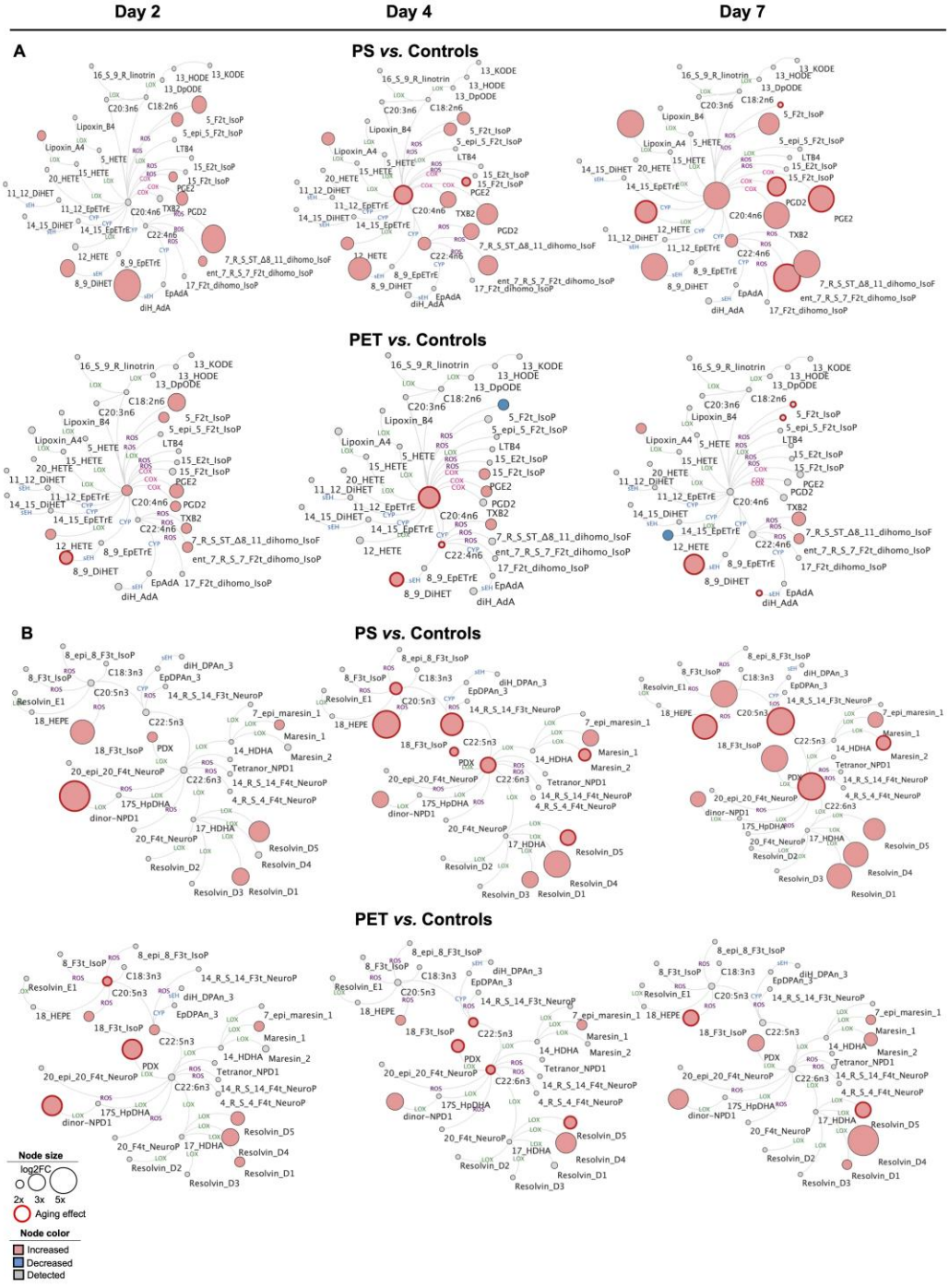


Figure 2. Temporal remodeling of n-6 (A) and n-3 (B) PUFA-derived oxylipin networks in cardiomyocyte media following exposure to virgin and aged polystyrene (PS) and polyethylene terephthalate (PET) at days 2, 4, and 7. Fold changes relative to controls are mapped onto metabolic pathways. Node size represents the magnitude of Log_2 FC, and node color indicates directionality

(salmon-pink, increased; blue, decreased; grey, not significantly altered). Only statistically significant metabolites are highlighted, while additional detected intermediates are shown in grey for context within the pathway. Enzymatic steps (e.g., LOX, COX, CYP) are indicated along edges. Red borders denote metabolites significantly affected by aging. The network illustrates time-dependent and polymer-specific alterations in lipid mediator pathways.

4. Discussion

This study shows that MPs do not induce a uniform cardiomyocyte response, but rather distinct polymer-, aging-, and time-dependent patterns of oxidative stress, lipid remodeling, inflammation, and resolution-associated lipid responses. Given the relatively large particle size, these effects may involve extracellular interactions and soluble polymer-derived leachates or photo-oxidation products. However, limited particle uptake cannot be excluded [38]. Dailianis et al. reported oxidative and cytogenotoxic effects of pristine and UV-B-aged LDPE particles in the 100–180 μm range, with pristine particles not detected as internalized in their model, and aging associated with altered particle morphology and surface chemistry [39]. These findings support the possibility that relatively large particles can remain biologically active without requiring efficient cellular uptake.

Importantly, by integrating cell viability, caspase-1 activity, PUFA remodeling, oxylipins, cytokines, and pro-resolving mediators, this study provides a broader picture of MP-induced cellular responses than approaches focused mainly on oxidative stress or inflammation.

Among the polymers tested, HDPE and PS produced the strongest oxylipin and PUFA remodeling, whereas LDPE showed the clearest effect of aging. Aged LDPE reduced cell viability by 38% and showed sustained elevations in PUFAs and SPMs, whereas a significant increase in caspase-1 activity was observed only with virgin LDPE. PET and HDPE also significantly increased caspase-1 activity, whereas PS did not, despite its marked oxylipin response. This apparent dissociation between lipid mediators, caspase-1 activity, and cytokines is mechanistically plausible because these outputs are regulated by partly independent upstream pathways. COX/LOX-derived oxylipin production depends on enzymatic activity and PUFA availability, whereas isoprostanes are generated non-enzymatically during lipid peroxidation [40]. In contrast, caspase-1 activation requires inflammasome assembly, while TNF-α and IL-6 production is regulated in part by NF-κB signaling.

PS provides the clearest example of this distinction, producing strong pro-inflammatory oxylipin responses without a significant increase in caspase-1 activity. Activation of the NLR family pyrin domain-containing 3 (NLRP3) inflammasome and caspase-1 by particulate stimuli generally depends on efficient cellular uptake and lysosomal damage [41]. Considering the particle size used here and the fact that cardiomyocytes are not professional phagocytes, this pathway may be less readily engaged. Thus, PS may promote membrane-level lipid peroxidation and eicosanoid production without triggering a significant increase in caspase-1 activity , despite evidence that PS can activate the NLRP3/caspase-1 pathway when efficient internalization occurs [41,42]. The limited PS inflammatory response is also consistent with recent evidence showing lower PS activity than PET and PP in human hiPSC-derived cells [43].

The PUFA changes further support a polymer-specific response. Rather than showing a uniform pattern, PUFA levels followed distinct temporal trajectories, with the strongest remodeling observed for HDPE and a sustained response in aged LDPE. These changes suggest that MPs can alter the availability of lipid substrates feeding downstream oxylipin pathways, highlighting lipid metabolism as a potentially active component of the cellular response rather than simply a consequence of cell damage. The most distinctive finding was the polymer- and time-dependent variation in extracellular SPM levels, SPMs did not simply parallel the inflammatory or oxidative response, but followed polymer-specific temporal patterns, with marked increases after HDPE and PS exposure and sustained elevation in aged LDPE, whereas PET showed a comparatively stable profile. This coexistence of inflammatory/oxidative and pro-resolving signals suggests that cardiomyocytes may actively engage resolution pathways in response to persistent lipid stress, rather than undergoing a

simple transition from inflammation to resolution [44]. Importantly, the divergence between lipid mediator responses and cytokines may also reflect active immunomodulation by the lipid network. SPMs can restrain NF-κB activation and inflammatory cytokine and ROS production [45,46], while PGE2 can suppress inflammatory signaling through EP2/EP4–cAMP pathways [47]. Accordingly, the conditions with the strongest oxylipin responses, particularly HDPE and PS, showed no significant changes in TNF-α, while IL-6 was reduced in both HDPE forms and virgin PS. PET, with a comparatively stable pro-resolving profile, showed increased IL-6. Thus, the term "pro-inflammatory" should be interpreted cautiously for individual lipid mediators, as several oxylipins can also exert context-dependent immunomodulatory effects.

LDPE provides the clearest example of the impact of photo-oxidative aging. Aging did not simply increase MP toxicity, but changed the cellular response profile, with aged LDPE showing reduced viability, sustained elevations in extracellular PUFAs, and elevated SPMs. This suggests that photo-oxidative aging may reshape the balance between cellular injury and resolution-associated lipid responses resolution rather than simply increasing the magnitude of toxicity.

A key strength of this study is therefore the direct comparison of virgin and aged polymers together with longitudinal assessment of multiple lipid mediator pathways. Much of the existing literature has examined pristine particles or individual inflammatory and oxidative endpoints, making it difficult to capture how polymer chemistry and aging influence the evolution of the cellular response. Here, the simultaneous assessment of stress-associated and potentially compensatory pathways provides a more comprehensive picture of cardiomyocyte responses to MP exposure and highlights changes in extracellular SPM levels as a relatively unexplored component of cardiovascular MP responses.

Several limitations should nevertheless be considered. First, the in vitro exposures were limited to seven days at a single concentration of 1 mg/mL and do not reproduce chronic human exposure. Moreover, environmental MPs occur as complex mixtures and may carry additives or co-pollutants that modify their biological effects [49]. Second, although changes in extracellular SPM levels provide new insight into resolution-associated lipid responses, whether these changes are protective or become dysfunctional during chronic exposure requires functional validation and in vivo confirmation. Finally, the PUFA and oxylipin changes are consistent with membrane perturbation and increased lipid turnover. Still membrane organization and biophysical properties were not directly measured and should be investigated in future studies.

Overall, these findings support a model in which polymer type, photo-oxidative aging, and exposure time influence not only the magnitude of cardiomyocyte stress, but also the balance between lipid oxidation, inflammation, and potentially compensatory lipid responses. The identification of changes in extracellular SPM levels adds a resolution-centered dimension that remains comparatively underexplored in cardiovascular MP toxicity. Future studies should determine whether this response is functionally protective and whether prolonged exposure ultimately overwhelms these putative endogenous mechanisms.

5. Conclusions

Photo-oxidative aging does not simply increase the toxicity of microplastics; it can modify their biological effects in a polymer-dependent manner. By integrating lipidomics, inflammatory markers, and cellular assays, this study shows that cardiomyocyte responses to photo-oxidatively aged microplastics vary with polymer type and are accompanied by distinct lipid mediator profiles. Our findings suggest that oxidative stress accompanies lipid remodeling in the most responsive polymers, whereas polymer-specific lipid mediator signatures may reflect differences in inflammatory and potentially adaptive responses. Together, these findings extend the characterization of microplastic effects on cardiomyocytes beyond conventional oxidative stress endpoints to include polymer- and aging-dependent lipid mediator remodeling.

Acknowledgements

This article is based on work from the Sample Preparation Task Force and Network, supported by the Division of Analytical Chemistry of the European Chemical Society.

References

[1] F. Prattichizzo, A. Ceriello, V. Pellegrini, R. La Grotta, L. Graciotti, F. Olivieri, P. Paolisso, B. D'Agostino, P. Iovino, M.L. Balestrieri, S. Rajagopalan, P.J. Landrigan, R. Marfella, G. Paolisso, Micro-nanoplastics and cardiovascular diseases: evidence and perspectives, Eur Heart J 45 (2024) 4099–4110. https://doi.org/10.1093/eurheartj/ehae552.

[2] D.-W. Lee, J. Jung, S. Park, Y. Lee, J. Kim, C. Han, H.-C. Kim, J.H. Lee, Y.-C. Hong, Microplastic particles in human blood and their association with coagulation markers, Sci Rep 14 (2024) 30419. https://doi.org/10.1038/s41598-024-81931-9.

[3] L.C. Jenner, J.M. Rotchell, R.T. Bennett, M. Cowen, V. Tentzeris, L.R. Sadofsky, Detection of microplastics in human lung tissue using μFTIR spectroscopy, Science of The Total Environment 831 (2022) 154907. https://doi.org/10.1016/j.scitotenv.2022.154907.

[4] A. Ragusa, A. Svelato, C. Santacroce, P. Catalano, V. Notarstefano, O. Carnevali, F. Papa, M.C.A. Rongioletti, F. Baiocco, S. Draghi, E. D'Amore, D. Rinaldo, M. Matta, E. Giorgini, Plasticenta: First evidence of microplastics in human placenta, Environ Int 146 (2021) 106274. https://doi.org/10.1016/j.envint.2020.106274.

[5] R. Marfella, F. Prattichizzo, C. Sardu, G. Fulgenzi, L. Graciotti, T. Spadoni, N. D'Onofrio, L. Scisciola, R.L. Grotta, C. Frigé, V. Pellegrini, M. Municinò, M. Siniscalchi, F. Spinetti, G. Vigliotti, C. Vecchione, A. Carrizzo, G. Accarino, A. Squillante, G. Spaziano, D. Mirra, R. Esposito, S. Altieri, G. Falco, A. Fenti, S. Galoppo, S. Canzano, F.C. Sasso, G. Matacchione, F. Olivieri, F. Ferraraccio, I. Panarese, P. Paolisso, E. Barbato, C. Lubritto, M.L. Balestrieri, C. Mauro, A.E. Caballero, S. Rajagopalan, A. Ceriello, B. D'Agostino, P. Iovino, G. Paolisso, Microplastics and Nanoplastics in Atheromas and Cardiovascular Events, New England Journal of Medicine 390 (2024) 900–910. https://doi.org/10.1056/NEJMoa2309822.

[6] Y. Yang, E. Xie, Z. Du, Z. Peng, Z. Han, L. Li, R. Zhao, Y. Qin, M. Xue, F. Li, K. Hua, X. Yang, Detection of Various Microplastics in Patients Undergoing Cardiac Surgery, Environ. Sci. Technol. 57 (2023) 10911–10918. https://doi.org/10.1021/acs.est.2c07179.

[7] J. Martín-Pérez, A. Villacorta, J. Gutiérrez-García, R. Egea, M. Morataya-Reyes, M. Cassú-Casadevall, I. Barguilla, R. Marcos, A. Hernández, A. García-Rodríguez, Transcriptomic and functional profiling of endothelial dysfunction induced by polystyrene nanoplastics, Front. Toxicol. 8 (2026). https://doi.org/10.3389/ftox.2026.1812922.

[8] N. Yang, B. Wu, X. He, J. Ma, L. Dai, R. Ma, T. Yang, X. Ning, X. Li, S. Jia, Polystyrene bead ingestion promotes atherosclerosis plaque progression via BMP signaling in mice, Food and Chemical Toxicology 202 (2025) 115455. https://doi.org/10.1016/j.fct.2025.115455.

[9] X. Zhu, C. Wang, X. Duan, B. Liang, E. Genbo Xu, Z. Huang, Micro- and nanoplastics: A new cardiovascular risk factor?, Environ Int 171 (2023) 107662. https://doi.org/10.1016/j.envint.2022.107662.

[10] G. Binda, G. Kalčíková, I.J. Allan, R. Hurley, E. Rødland, D. Spanu, L. Nizzetto, Microplastic aging processes: Environmental relevance and analytical implications, TrAC Trends in Analytical Chemistry 172 (2024) 117566. https://doi.org/10.1016/j.trac.2024.117566.

[11] V. Castelvetro, A. Corti, G. Biale, A. Ceccarini, I. Degano, J. La Nasa, T. Lomonaco, A. Manariti, E. Manco, F. Modugno, V. Vinciguerra, New methodologies for the detection, identification, and quantification of microplastics and their environmental degradation by-products, Environ Sci Pollut Res 28 (2021) 46764–46780. https://doi.org/10.1007/s11356-021-12466-z.

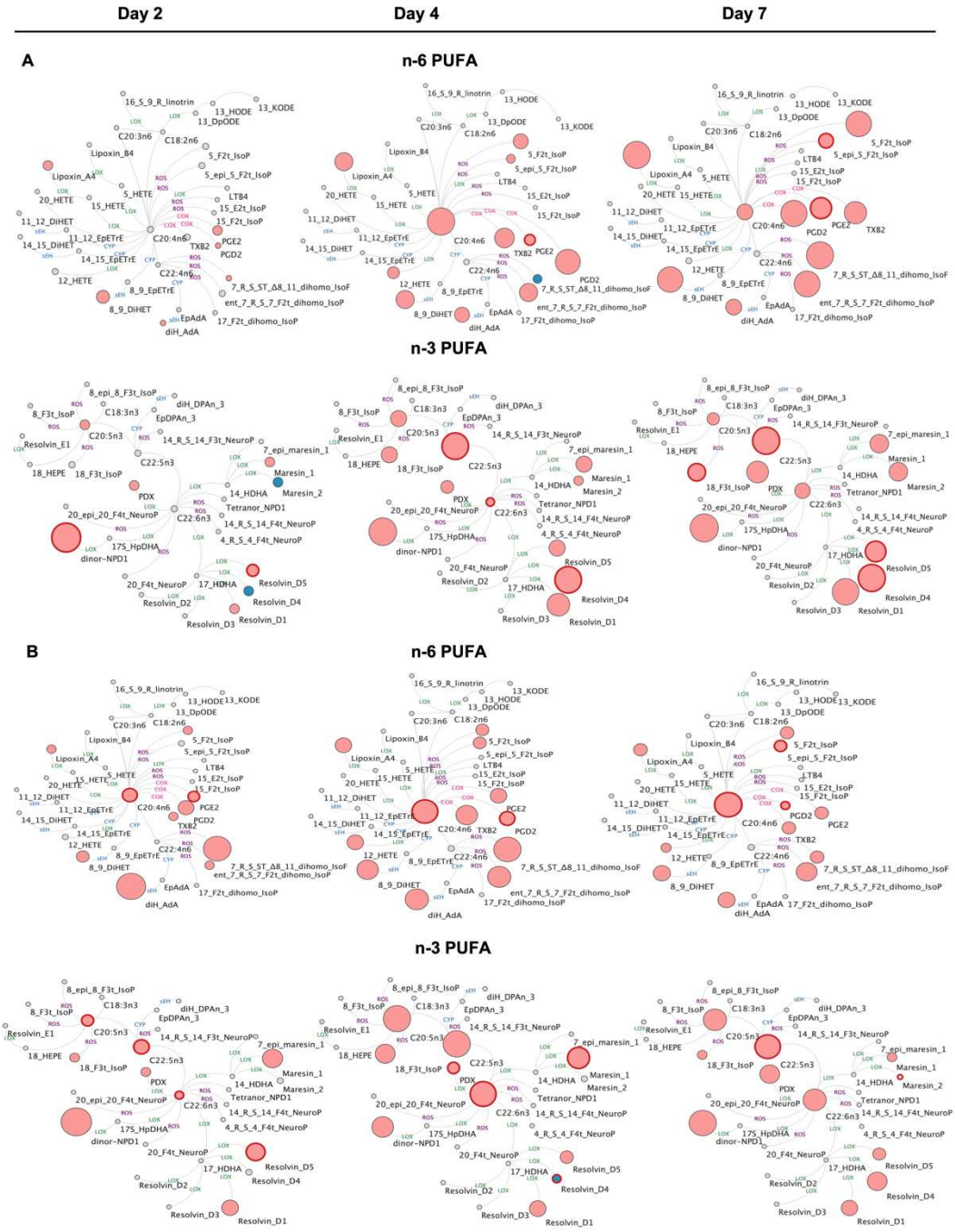
[12] T. Lomonaco, E. Manco, A. Corti, J. La Nasa, S. Ghimenti, D. Biagini, F. Di Francesco, F. Modugno, A. Ceccarini, R. Fuoco, V. Castelvetro, Release of harmful volatile organic compounds

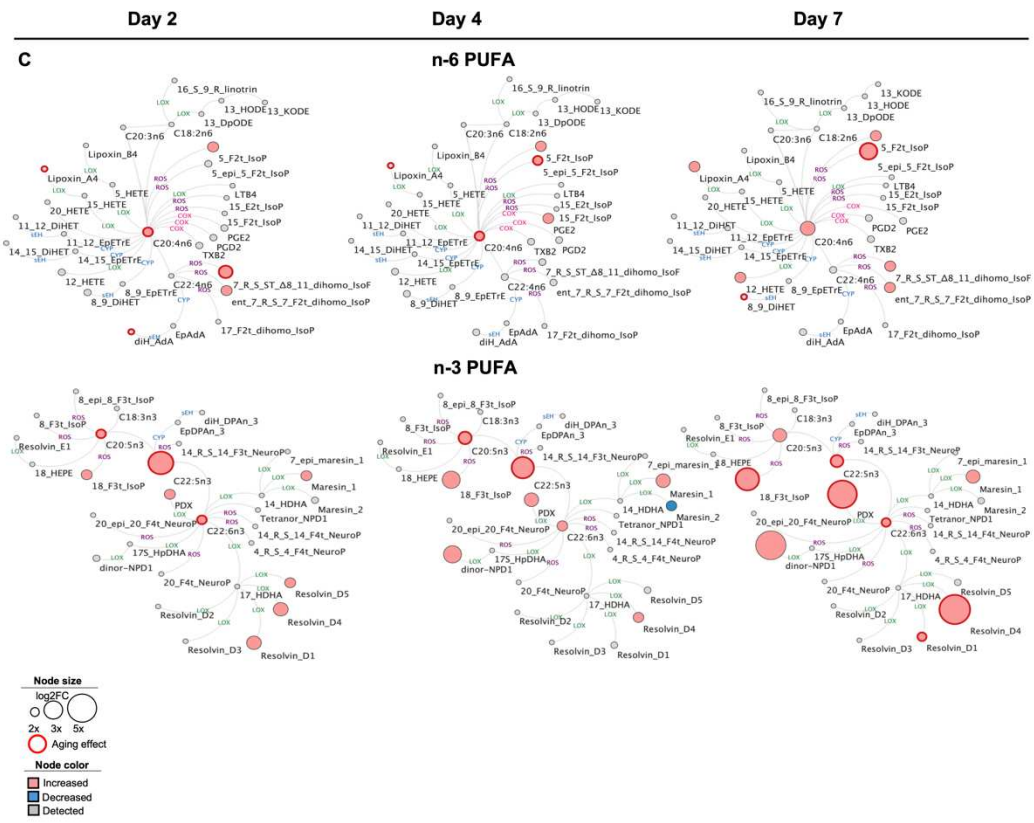
(VOCs) from photo-degraded plastic debris: A neglected source of environmental pollution, Journal of Hazardous Materials 394 (2020) 122596. https://doi.org/10.1016/j.jhazmat.2020.122596.
[13] J. La Nasa, T. Lomonaco, E. Manco, A. Ceccarini, R. Fuoco, A. Corti, F. Modugno, V. Castelvetro, I. Degano, Plastic breeze: Volatile organic compounds (VOCs) emitted by degrading macro- and microplastics analyzed by selected ion flow-tube mass spectrometry, Chemosphere 270 (2021) 128612. https://doi.org/10.1016/j.chemosphere.2020.128612.
[14] E. Murphy, C. Steenbergen, Mechanisms underlying acute protection from cardiac ischemia-reperfusion injury, Physiol Rev 88 (2008) 581–609. https://doi.org/10.1152/physrev.00024.2007.
[15] M.R. Bornstein, R. Tian, Z. Arany, Human cardiac metabolism, Cell Metabolism 36 (2024) 1456–1481. https://doi.org/10.1016/j.cmet.2024.06.003.
[16] T.-H. Chen, I.-T. Chu, R.-Y. Chang, H.-C. Wang, C.-J. Chung, T.-H. Tsai, C.-K. Chou, Microplastics induce mitochondrial dysfunction and accelerate cardiovascular pathogenesis, Arch Toxicol 100 (2026) 1699–1711. https://doi.org/10.1007/s00204-026-04327-w.
[17] C.N. Serhan, Pro-resolving lipid mediators are leads for resolution physiology, Nature 510 (2014) 92–101. https://doi.org/10.1038/nature13479.
[18] J. Dalli, C.N. Serhan, Pro-Resolving Mediators in Regulating and Conferring Macrophage Function, Front Immunol 8 (2017) 1400. https://doi.org/10.3389/fimmu.2017.01400.
[19] A.M. Astudillo, M.A. Balboa, J. Balsinde, Compartmentalized regulation of lipid signaling in oxidative stress and inflammation: Plasmalogens, oxidized lipids and ferroptosis as new paradigms of bioactive lipid research, Progress in Lipid Research 89 (2023) 101207. https://doi.org/10.1016/j.plipres.2022.101207.
[20] C. Li, Z. Wang, Y. Yang, Q. Jiang, Y. Jiang, J. Xiao, L. Shen, W. Wu, C. Li, Pro-resolving lipid mediators in diseases: exploring the molecular basis and clinical implication, Mol Biomed 7 (2026) 1. https://doi.org/10.1186/s43556-025-00400-5.
[21] C.N. Serhan, S. Yacoubian, R. Yang, Anti-Inflammatory and Pro-Resolving Lipid Mediators, Annu Rev Pathol 3 (2008) 279–312. https://doi.org/10.1146/annurev.pathmechdis.3.121806.151409.
[22] N.H. Schebb, N. Kampschulte, G. Hagn, K. Plitzko, S.W. Meckelmann, S. Ghosh, R. Joshi, J. Kuligowski, D. Vuckovic, M.T. Botana, Á. Sánchez-Illana, F. Zandkarimi, A. Das, J. Yang, L. Schmidt, A. Checa, H.M. Roche, A.M. Armando, M.L. Edin, F.B. Lih, J.J. Aristizabal-Henao, S. Miyamoto, F. Giuffrida, A. Moussaieff, R. Domingues, M. Rothe, C. Hinz, U.S. Das, K.M. Rund, A.Y. Taha, R.K. Hofstetter, M. Werner, O. Werz, A.S. Kahnt, J. Bertrand-Michel, P. Le Faouder, R. Gurke, D. Thomas, F. Torta, I. Milic, I.H.K. Dias, C.M. Spickett, D. Biagini, T. Lomonaco, H. Idborg, J.-Y. Liu, M. Fedorova, D.A. Ford, A. Barden, T.A. Mori, P.D. Kennedy, K. Maxey, J. Ivanisevic, H. Gallart-Ayala, C. Gladine, M. Wenk, J.-M. Galano, T. Durand, K.D. Stark, C. Barbas, U. Garscha, S.L. Gelhaus, U. Ceglarek, N. Flamand, J.L. Griffin, R. Ahrends, M. Arita, D.C. Zeldin, F.J. Schopfer, O. Quehenberger, R. Julian, A. Nicolaou, I.A. Blair, M.P. Murphy, B.D. Hammock, B. Freeman, G. Liebisch, C.N. Serhan, H.C. Köfeler, P.-J. Jakobsson, D. Steinhilber, M.H. Gelb, M. Holčapek, R. Andrew, M. Giera, G.A. FitzGerald, R.C. Murphy, J.W. Newman, E.A. Dennis, K. Ekroos, G.L. Milne, M.A. Gijón, H.W. Vesper, C.E. Wheelock, V.B. O'Donnell, Technical recommendations for analyzing oxylipins by liquid chromatography-mass spectrometry, Sci Signal 18 (2025) eadw1245. https://doi.org/10.1126/scisignal.adw1245.
[23] P. Korram, T. Satapathy, From signal amplification to inflammatory resolution: The NF-κB-inflammasome-SPM axis as an integrated regulatory network, TransMed 1 (2026) 100038. https://doi.org/10.1016/j.tmed.2026.100038.
[24] C. Oger, Y. Brinkmann, S. Bouazzaoui, T. Durand, J.-M. Galano, Stereocontrolled access to isoprostanes via a bicyclo[3.3.0]octene framework, Org Lett 10 (2008) 5087–5090. https://doi.org/10.1021/ol802104z.

[25] L. Balas, P. Risé, D. Gandrath, G. Rovati, C. Bolego, F. Stellari, A. Trenti, C. Buccellati, T. Durand, A. Sala, Rapid Metabolization of Protectin D1 by β-Oxidation of Its Polar Head Chain, J. Med. Chem. 62 (2019) 9961–9975. https://doi.org/10.1021/acs.jmedchem.9b01463.
[26] I. Gisone, M. Boffito, E. Persiani, R. Pappalardo, E. Ceccherini, A. Alliaud, M. Cabiati, R. Laurano, L. Guiducci, C. Caselli, R. Ragusa, C. Cassino, C. Ippolito, S. Del Ry, S. Sartori, A. Cecchettini, S. Fernández-Arroyo, G. Ciardelli, F. Vozzi, Integration of co-culture conditions and 3D gelatin methacryloyl hydrogels to improve human-induced pluripotent stem cells-derived cardiomyocytes maturation, Front. Bioeng. Biotechnol. 13 (2025). https://doi.org/10.3389/fbioe.2025.1576824.
[27] Y.-L. Wang, Y.-H. Lee, Y.-H. Hsu, I.-J. Chiu, C.C.-Y. Huang, C.-C. Huang, Z.-C. Chia, C.-P. Lee, Y.-F. Lin, H.-W. Chiu, The Kidney-Related Effects of Polystyrene Microplastics on Human Kidney Proximal Tubular Epithelial Cells HK-2 and Male C57BL/6 Mice, Environ Health Perspect 129 (2021) 057003. https://doi.org/10.1289/EHP7612.
[28] W.A. Yehye, N.A. Rahman, A. Ariffin, S.B. Abd Hamid, A.A. Alhadi, F.A. Kadir, M. Yaeghoobi, Understanding the chemistry behind the antioxidant activities of butylated hydroxytoluene (BHT): a review, Eur J Med Chem 101 (2015) 295–312. https://doi.org/10.1016/j.ejmech.2015.06.026.
[29] D. Biagini, S. Ghimenti, A. Lenzi, A. Bonini, F. Vivaldi, C. Oger, J.-M. Galano, L. Balas, T. Durand, P. Salvo, F. Di Francesco, T. Lomonaco, Salivary lipid mediators: Key indexes of inflammation regulation in heart failure disease, Free Radical Biology and Medicine 201 (2023) 55–65. https://doi.org/10.1016/j.freeradbiomed.2023.03.015.
[30] D. Biagini, M. Franzini, P. Oliveri, T. Lomonaco, S. Ghimenti, A. Bonini, F. Vivaldi, L. Macera, L. Balas, T. Durand, C. Oger, J.-M. Galano, F. Maggi, A. Celi, A. Paolicchi, F. Di Francesco, MS-based targeted profiling of oxylipins in COVID-19: A new insight into inflammation regulation, Free Radical Biology and Medicine 180 (2022) 236–243. https://doi.org/10.1016/j.freeradbiomed.2022.01.021.
[31] M. Thompson, S.L.R. Ellison, R. Wood, Harmonized Guidelines for Single-Laboratory Validation of Methods of Analysis: (IUPAC Technical Report), (n.d.). https://doi.org/10.1515/iupac.74.0084.
[32] R.F. Martin, General deming regression for estimating systematic bias and its confidence interval in method-comparison studies, Clin Chem 46 (2000) 100–104.
[33] J. Sun, Y. Xia, Pretreating and normalizing metabolomics data for statistical analysis, Genes & Diseases 11 (2024) 100979. https://doi.org/10.1016/j.gendis.2023.04.018.
[34] D.D. Krutkin, S. Thomas, S. Zuffa, P. Rajkumar, R. Knight, P.C. Dorrestein, S.T. Kelley, To Impute or Not To Impute in Untargeted Metabolomics─That is the Compositional Question, J. Am. Soc. Mass Spectrom. 36 (2025) 742–759. https://doi.org/10.1021/jasms.4c00434.
[35] P. Oliveri, C. Malegori, R. Simonetti, M. Casale, The impact of signal pre-processing on the final interpretation of analytical outcomes – A tutorial, Analytica Chimica Acta 1058 (2019) 9–17. https://doi.org/10.1016/j.aca.2018.10.055.
[36] Y. Benjamini, Y. Hochberg, Controlling the False Discovery Rate: A Practical and Powerful Approach to Multiple Testing, Journal of the Royal Statistical Society. Series B (Methodological) 57 (1995) 289–300.
[37] P. Shannon, A. Markiel, O. Ozier, N.S. Baliga, J.T. Wang, D. Ramage, N. Amin, B. Schwikowski, T. Ideker, Cytoscape: a software environment for integrated models of biomolecular interaction networks, Genome Res 13 (2003) 2498–2504. https://doi.org/10.1101/gr.1239303.
[38] J. Rejman, V. Oberle, I.S. Zuhorn, D. Hoekstra, Size-dependent internalization of particles via the pathways of clathrin- and caveolae-mediated endocytosis., Biochem J 377 (2004) 159–169. https://doi.org/10.1042/BJ20031253.
[39] S. Dailianis, M. Rouni, N.M. Ainali, D. Vlastos, G.Z. Kyzas, D.A. Lambropoulou, D.N. Bikiaris, New insights into the size-independent bioactive potential of pristine and UV-B aged

polyethylene microplastics, Sci Total Environ 918 (2024) 170616. https://doi.org/10.1016/j.scitotenv.2024.170616.
[40] S. Basu, Isoprostanes: novel bioactive products of lipid peroxidation, Free Radic Res 38 (2004) 105–122. https://doi.org/10.1080/10715760310001646895.
[41] J. Wei, X. Wang, Q. Liu, N. Zhou, S. Zhu, Z. Li, X. Li, J. Yao, L. Zhang, The impact of polystyrene microplastics on cardiomyocytes pyroptosis through NLRP3/Caspase-1 signaling pathway and oxidative stress in Wistar rats, Environmental Toxicology 36 (2021) 935–944. https://doi.org/10.1002/tox.23095.
[42] Y. Mu, J. Sun, Z. Li, W. Zhang, Z. Liu, C. Li, C. Peng, G. Cui, H. Shao, Z. Du, Activation of pyroptosis and ferroptosis is involved in the hepatotoxicity induced by polystyrene microplastics in mice, Chemosphere 291 (2022) 132944. https://doi.org/10.1016/j.chemosphere.2021.132944.
[43] H. Brouwer, M. Busch, S. Yang, T. Venus, G. Aalderink, J.F.F. Crespo, A. Villacorta, A. Hernández, I. Estrela-Lopis, S. Boeren, H. Bouwmeester, Toxicity of true-to-life microplastics to human iPSC-derived intestinal epithelia correlates to their protein corona composition, J Hazard Mater 495 (2025) 138908. https://doi.org/10.1016/j.jhazmat.2025.138908.
[44] C.D. Buckley, D.W. Gilroy, C.N. Serhan, B. Stockinger, P.P. Tak, The resolution of inflammation, Nat Rev Immunol 13 (2013) 59–66. https://doi.org/10.1038/nri3362.
[45] P. Singer, H. Shapiro, M. Theilla, R. Anbar, J. Singer, J. Cohen, Anti-inflammatory properties of omega-3 fatty acids in critical illness: novel mechanisms and an integrative perspective, Intensive Care Med 34 (2008) 1580–1592. https://doi.org/10.1007/s00134-008-1142-4.
[46] J. Dong, M. Zhang, Z. Liao, W. Wu, T. Wang, L. Chen, T. Yang, L. Guo, D. Xu, F. Wen, Resolvin-D1 inhibits interleukin-8 and hydrogen peroxide production induced by cigarette smoke extract in 16HBE cells via attenuating NF-κB activation, Chin Med J (Engl) 127 (2014) 511–517.
[47] X.J. Xu, J.S. Reichner, B. Mastrofrancesco, W.L. Henry, J.E. Albina, Prostaglandin E2 suppresses lipopolysaccharide-stimulated IFN-beta production, J Immunol 180 (2008) 2125–2131. https://doi.org/10.4049/jimmunol.180.4.2125.

Supplementary info





Supplementary Figure 1. Temporal remodeling of n-6 and n-3 PUFA-derived oxylipin networks in cardiomyocyte media following exposure to virgin and aged HDPE (**A**), LDPE (**B**), and PP (**C**) at days 2, 4, and 7. Fold changes relative to control cultures were mapped onto oxylipins metabolic pathways. Node size represents the magnitude of the Log_2 FC, and node color indicates the direction of regulation (salmon-pink, increased; blue, decreased; grey, not significantly altered). Statistically significant metabolites are highlighted in color, whereas detected but non-significant metabolites are shown in grey to preserve pathway context. Enzymatic conversions mediated by LOX, COX, CYP, and related pathways are indicated along the connecting edges. Metabolites significantly affected by polymer aging are outlined in red. The network reveals both time-dependent and polymer-specific alterations in lipid mediator pathways.